Design of a Charge Sustaining Energy Management System for a Free-Floating Electric Shared Bicycle

Matteo Corno[1], Alessandra Duz[1], and Sergio M. Savaresi[1]

***Abstract*—This paper proposes an energy management system (EMS) for shared electric bicycles.The objective is to guarantee electric assistance to the cyclist while avoiding discharging the battery. The basic working principle exploits the cycling efficiency gaps.**

The proposed multi-layered EMS is specifically tailored to a free-floating bike sharing setting. The innermost layer manages the assistance and energy harvesting with the objective of yielding an intuitive human-machine interface. The middle level modulates the level of assistance so to track a desired average battery power. This is an adaptive model-based controller designed on a control-oriented model of the cyclist and bicycle energy dynamics. A cyclist profiling mechanism enables the model adaptation. The outermost loop guarantees the long term robustness by tracking a desired battery state of charge profile.

Extensive simulations and experimental tests validate this approach in terms of usability and charge sustenance, proving that the cyclist profiling is of paramount importance.

I. Introduction

Privately owned fossil-based mobility has shown over and over not to be sustainable. Shared mobility and light electric vehicles (LEV) could represent a viable alternative. Shared mobility, *i.e.* the availability of a fleet of vehicles that can be rented on the go, could reduce congestion. LEV's offer more energy-efficient means of transportation. Many cities are actively promoting electric vehicle sharing in the shape of shared electric scooters, moped, and cars.

One of the most successful vehicle sharing system in European and Asian cities is bike-sharing. Bicycles have many advantages; they are efficient, green and promote a healthy life style. Bicycles are however not viable for everyone as they require a certain level of physical fitness. The introduction of a bike sharing system based on Electrically Power Assisted Cycles (EPAC) could enlarge the user basin. In EPAC's, an electric motor provide assistance while cycling [1]–[4], thus reducing the cyclist's physical effort.

There exist two types of bike sharing systems: station-based and free-floating. In station-based systems, bicycles are parked (picked and returned) at fixed stalls. In free-floating systems, bicycles are freely parked and picked-up in a predefined geographical area [5].

Station-based bike sharing systems are relatively easy to electrify: the stalls can be equipped with a charging system that keeps the bicycles charged. The task is more complex for free-floating systems where normally bicycles are maintained by a team of employees. Recharging the bicycles considerably increases operational costs.

This paper discusses the application of charge-sustaining control to electric bikes designed to operate in a sharing system. In particular, we extend the concept of the charge sustaining full hybrid electric bicycle (HEB), whose potential has been already assessed in [6]–[8], to bike sharing applications. Charge sustaining HEB's exploit the gaps in the cyclist's pedaling efficiency to guarantee a zero net battery energy consumption and a reduction of the cyclist's pedaling effort. The idea of charge sustaining HEB's stems from the work on hybrid-electric vehicles ([9], [10]). Designing an energy management system for hybrid bicycles follows the same rationale as in traditional hybrid-electric vehicles, but there are differences that set the problem aside and prevent the application of well-proven techniques like the equivalent consumption minimization strategy [11]. The two most important differences are the fact that the primary mover's (*i.e.* the cyclist) efficiency cannot be modeled with static maps and the fact that the pedals are at the same time a user-machine interface and a power flow path, see also [12], [13] for more a more detailed comparison between hybrid bicycles and other vehicles.

The existing literature on the topic examines private bike usage. The integration of HEB's in a bike sharing scenario poses new challenges:

- bike sharing systems need to track and manage the renting of the vehicles; each bicycle is equipped with additional electronics that considerably change the electric power absorption profiles with respect to private use. In particular, the absorption while the bicycle is not being used cannot be neglected.
- the typical use of a vehicle in a bike sharing context is very different from the use of a private bicycle: by definition, a shared bicycle is used by a number of different users; the average trip is considerably shorter than in private use and the mission profiles have a larger variability than in private use.

These factors call for a complete redesign of the bicycle energy management system. This paper designs a novel energy management system for a HEB designed to be integrated in a bike sharing system. In particular:

- We define a method to quantitatively profile, from the energy point of view, the users of the sharing system.
- We develop a causal and adaptive EMS for shared bicycles. The EMS aims at providing assistance while avoiding battery charge depletion. The EMS uses the cyclists' profiles to adapt to each cyclists' characteristics.
- We validate the approach on data collected during a trial

[1] M. Corno, A. Duz, and S.M. Savaresi are with Dipartimento di Elettronica Informazione e Bioingegneria at Politecnico di Milano, e-mail: matteo.corno@polimi.it , alessandra.duz@polimi.it, and sergio.savaresi@polimi.it. This work has been supported by Zehus SpA and by the European Union under the Funding Scheme SME-2 - SME instrument phase 2 - Grant agreement ID: 756656

in the City of Milan of an electric free-floating bicycle sharing system.

We stress that the focus is on the bicycle-level EMS; as it will become clear later, the bicycle is only one, although critical, element of a bike sharing system. Having an effective EMS is only a necessary condition for the economic sustainability of a bicycle sharing system.

The paper is structured as follows: Section II and Section III describe the bicycle, and its simulator respectively; Section IV details the adaptive energy management system. Section V validates the system, both in simulation and experimentally. Finally, Section VI draws the relevant conclusions.

II. Electric Shared Bike Description

This section describes the characteristics of the reference bicycle in the context of a free-floating bike sharing scenario.

The bicycle is build around a city bike frame (see Figure 1) equipped with an All in One (AiO) powertrain and additional items for managing the renting process. The AiO contains:

- A Brushless DC motor (with a nominal power of 250 W).
- A 160 Wh Li-ion battery pack with its Battery Management System (BMS). The BMS implements safety checks and estimates the battery state of charge as explained in [14].
- An Inertial Measurement Unit (IMU), that, among other tasks, estimates the road slope using the results of [15].
- A programmable Electric Control Unit (ECU).
- Pedaling cadence sensor.
- Motor Speed sensor.

The powertrain is the same as the one discussed in [6], [8]. Note that the bicycle is not equipped with a pedaling torque sensor. In addition, an electronic box enables the rental process. This *sharing box* contains:

- a GPS system for tracking the bicycle position.
- A cellular network communication unit.
- An electro-mechanical lock.

These components draw power both during the ride and while idling between rentals. The rental process consists of the following steps:

Fig. 1. The bicycles used in this study.

1) the user logs on the service. The service tracks all the bicycles and the user's app shows their position on a map.
2) The user reaches the closest bike.
3) The user unlocks the bike through a cloud request and starts the ride.
4) Once the user has reached her destination, she releases the bike by locking it manually. The bicycle connects to the cloud and communicates the end of the rental.

Note that the communication between the bicycle and the user always happens through the internet.

III. System Modeling

This section proposes a model of the human-bicycle system. The focus of the model is on the power fluxes. We organize the discussion in several components: vehicle dynamics, powertrain dynamics, trip dynamics and cyclist dynamics.

A. Vehicle dynamics

The model focuses on the longitudinal dynamics of the vehicle, as the ones that mainly affect energy efficiency and consumption ([16]). The force balance is:

$$\begin{aligned} M\dot{v} &= F_g(\theta) + F_\mu(v) + (T_c + T_m - T_b)r \\ F_g &= -Mg\sin(\theta) \\ F_\mu &= -\frac{1}{2}\rho C_x A v_w^2 - D_v v - C_r Mg\cos(\theta). \end{aligned}$$

where M is the total equivalent mass of the bicycle and of the cyclist, v is the longitudinal bicycle speed with respect to the ground, v_w is the longitudinal bicycle speed with respect to the wind, ρ is the air density, A is the front area of the bicycle and of the cyclist, C_x is the drag coefficient, D_v is the mechanical friction coefficient, θ is the road slope (positive uphill), r is the wheel rolling radius, C_r is the rolling friction coefficient, T_c is the traction torque delivered by the cyclist at the wheel (only positive), T_b is the braking torque delivered by mechanical brake (only negative), and T_m the wheel torque generated by the motor (that can be both positive - assistive - and negative - regenerative). The model parameters are either measured (mass, wheel radius and slope) or identified from coasting down experiments (see [8], [17]).

B. Powertrain dynamics

Figure 2 depicts the system power flows. The battery power,

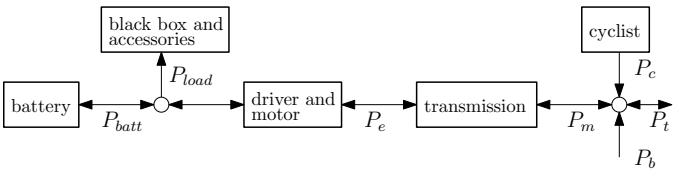

Fig. 2. Schematic representation of the power flows during the ride.

P_{batt}, is the sum of the power consumed by the loads P_{load} and the power absorbed (or generated) by the motor driver that controls the motor. P_e represents the electrical power of the motor, with P_m its mechanical counterpart at the wheel. P_c is the mechanical power produced by the cyclist. The sum of P_m, P_c and the friction brakes power gives the resulting traction

power, P_t, defined at the wheel. These power contributions can be quantified as:

$$P_m = T_m \omega$$
$$T_m = k_e I_m$$
$$P_{batt} = I_{batt} V_{batt}$$

where k_e (1.2 [Nm/A]) is the motor constant, I_m and I_{batt} the motor and battery currents, ω the wheel (and motor) angular rate and V_{batt} the battery voltage. Further, by accounting for the efficiencies of the transmission (η_{gear}) and of the driver (η) and defining positive a flow that discharges the battery:

$$P_m = \begin{cases} P_e \eta_{gear} & \text{if } P_e \geq 0 \\ \frac{P_e}{\eta_{gear}} & \text{if } P_e < 0 \end{cases}$$

$$P_{batt} = \begin{cases} P_e \eta + P_{load} & \text{if } P_e < 0 \\ \frac{P_e}{\eta} + P_{load} & \text{if } P_e \geq 0 \end{cases} .$$

Figure 3 plots the efficiency of the electrical machine and electrical driver as obtained from experiments on a test bench.

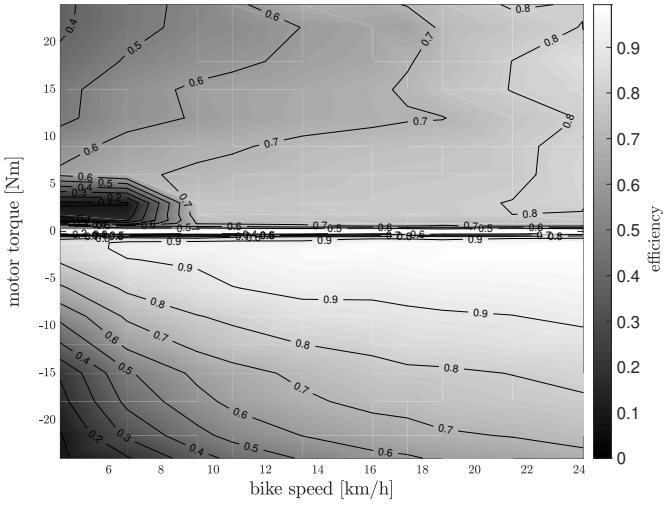

Fig. 3. Battery to Wheel efficiency for the electrical machine and drivers

.

Similarly, measurements on the accessories and the sharing-box reveal that P_{load} is 2.5 [W] when the bicycle is used and 0.3 [W] when the bicycle is not being used. The difference is due to the fact that, when the bicycle is not rented, the communication frequency with the back-end is reduced and other loads (lights) are turned off.

We model the State of Charge (SoC) of the battery, *i.e.* the ratio between residual energy and the battery capacity, with a Coulomb counting approach:

$$SoC(t) = SoC(0) - \frac{100}{3600} \frac{\int_{t_0}^{t} I_{batt}(\tau) d\tau}{Q_0}$$

where Q_0 is the total battery capacity in Ampere hour.

Figure 4 validates the electrical model by comparing the measured and simulated battery current and SoC given the requested motor torque during a 20 minutes trial. As the plots show, the model accurately describes the dynamics of the

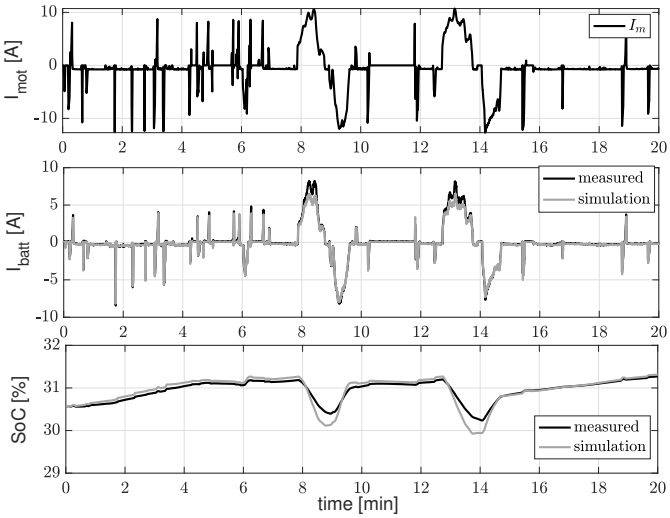

Fig. 4. Powertrain model validation. From top to bottom: motor current (input to the model), battery current and State of Charge dynamics.

battery current and SoC in the conditions of interest. Note that the SoC shows larger errors during high power requests as it is an integral quantity.

C. Trip dynamics

While the powertrain efficiency plays an important role, the bicycle power absorption mainly depends on the bicycle usage. In order to model this aspect, we develop a stochastic trip generator. The trip generator computes a velocity profile and a velocity controller, that represents the cyclist, tracks it. The stochastic trip generator takes as input a trip duration and a cyclist type and outputs a velocity and slope profiles.

The trip generator combines 9 primitive maneuvers. The primitive maneuvers are {*hard start, soft start, constant speed, coasting down, stop, hard braking, soft braking, hard sprint, soft sprint*}. Each maneuver, with the exception of the start and coasting down maneuvers, is characterized by a constant acceleration and a range of permissible final speeds. The coasting down maneuver follows the acceleration profile given by the friction acting on the bicycle; the start maneuvers are instead characterized by a time-varying acceleration profile that starts with a peak and returns to zero with a settling time of 4 seconds.

Given these primitive maneuvers, the trip generation algorithm executes the following steps:

1) the algorithm generates a sequence of primitives. The primitive maneuvers are the nodes of a Markov Chain that describes the probability of transitioning from one maneuver to another and guarantees that only feasible transitions are generated (*e.g.* the transition from stop to braking is meaningless) (see [18]).
2) The algorithm computes the duration of each maneuver in the sequence. For the maneuvers with a non null acceleration, the algorithm samples the final speed as a random variable uniformly distributed in the final speed range of that maneuver and determines the duration

needed to reach the speed at the prescribed acceleration. For the maneuvers with null acceleration, the algorithm directly samples a duration from a uniform distribution.
3) The algorithm adds maneuvers until the desired trip time is reached; at that point a final soft braking maneuver is generated to bring the bicycle to a full stop.
4) The algorithm adds a further random (white noise) component and filters the results with a low pass filter at 0.8 Hz to avoid discontinuities.
5) The algorithm computes a road slope for each *constant speed* maneuver. Note that we decided to assign a possibly non-zero road slope only to constant velocity tracts because, only rarely, in an urban setting, the cyclists change their speed on a slope.

In the above approach, the acceleration levels and the final speed for each maneuver type are user dependent. We consider three types of users: (sedentary, fit and athletic). We tuned the generator to reproduce the typical usage profile recorded during the trial of the free floating service.

Figure 5 shows the comparison between the velocity and the slope recorded during one of the trips of the trial and one of the trips generated by the trip generation algorithm. The

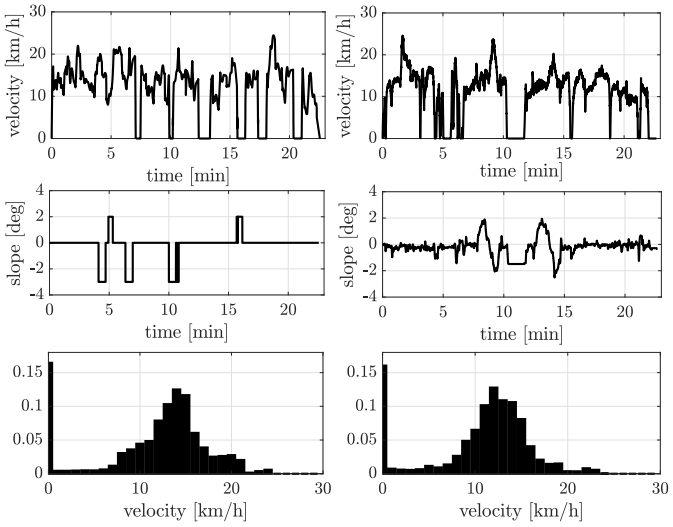

Fig. 5. Comparison between a generated trip (on the left) and a recorded trip (on the right). From top to bottom: bicycle speed, slope and velocity distribution.

goal of the trip generation algorithm is not that of replicating a recorded profile, but rather that of generating different velocity profiles that are realistic so to avoid overfitting in the tuning and validation phase. Further note that the algorithm focuses on generating single trips, it does not take into account pick up frequency and distribution throughout the day and the week.

D. Cyclist dynamics

The final component of the model is the cyclist. The cyclist's model serves two roles:

1) it acts as a velocity controller that tracks the speed reference.
2) It provides a way to compute the cyclist's pedaling effort.

The velocity controller generates T_c and T_b based on the velocity difference between the simulated velocity and the reference one. This controller thus considers both pedaling torque and braking actions. We assume that the two actions are mutually exclusive, either the cyclist brakes or pedals. Only the pedaling torque T_c plays a role in the subsequent effort considerations.

The assessment of cycling effort and cyclist fatigue are extensively addressed in literature and involve many different aspect of human physiology (see for example [19]–[23] [19], [24], [25]). The most accurate method requires the measurement of the instantaneous flow of O_2 and blood lactate. This approach does not provide a simulation model and is not practical in large trials. We therefore opted for two numerical indexes whose evaluation does not need additional equipment: the variance of the pedaling torque $var(T_c)$ and the cyclist's State of Fatigue (SoF).

1) Load variations: Variations of the pedaling torque generate a loss of equivalent pedaling efficiency (as discussed in [26]). The pedaling torque variance over a trip quantifies these variations. Despite $var(T_c)$ not being a direct measurement of the cycling efficiency, it is strictly correlated to it and thus can be used for relative comparisons.

2) State of Fatigue: The second index models the State of Fatigue ([24], [27]–[30]). Fatigue is defined as the reversible inability to maintain a muscular force output. Mathematically, we define

$$SoF(t) = \frac{MVC - F_{max}(t)}{MVC - F_{th}(t)}. \tag{1}$$

MVC is the *Maximum Voluntary Contraction* (MVC), that is the maximum force that a subject can apply when fully rested as a function of pedaling cadence ([31], [32]). It can be computed as in:

$$MVC_\omega = MVC\left(1 - \frac{\omega_{ped}(t)}{\omega_{max}}\right) \tag{2}$$

where ω_{ped} is the cyclist pedaling cadence and ω_{max} the maximum pedaling frequency (this value is found to be 190 RPM in [24]). F_{max} is the instantaneous force that a subject can apply at a given instant of the exercise. As the subject's fatigue accumulates, her instantaneous maximum force, F_{max}, drops below MVC_ω. A dynamic balance between effort and resting determines F_{max} according to

$$\frac{dF_{max}(t)}{dt} = -kF_{max}(t)\frac{F_{cyclist}(t)}{MVC_\omega} + R\left(MVC_\omega - F_{max}(t)\right) \tag{3}$$

where k the fatigue dynamic constant and R determines the resting dynamics. For a given contraction velocity, (3) admits an equilibrium called F_{th}:

$$F_{th} = MVC_\omega \frac{R}{2k}\left(-1 + \sqrt{1 + d\frac{k}{R}}\right).$$

Hence, F_{th} represents the lowest level of steady state force that the cyclist can produce indefinitely.

According to the previous considerations, and analyzing (2), one should note that

- The SoF is the normalized residual maximum force that the cyclist can apply.
- The rate of increase of SoF depends on the pedaling cadence; the higher the cadence is, the faster the increase of SoF at a given force is.
- The rate of increase of SoF depends on the force; the greater the force, the faster the increase of SoF.
- The model is dynamic, it is thus more descriptive than pedaling efficiency static maps.

The SoF is a dynamic index; comparing SoF values at certain time instants is not meaningful. The introduction of an integral quantity overcomes this limitation:

$$\xi = \frac{1}{T}\int_0^T 9 \cdot SoF(t)^2 + SoF(t)dt. \tag{4}$$

The cost function integrates a second order polynomial function of the SoF. The quadratic dependence accounts for the fact that cyclists would rather pedal at a steady SoF rather than having peaks and subsequent resting periods yielding the same average SoF. We use the same polynomial coefficients employed in [8] that give more relevance to the quadratic term; this choice enables an easier comparison with the available literature.

The SoF model has two main limitations. Primarily, it does not model a measurable quantity but an abstraction. Secondarily, it depends on a set of parameters that are not easily identified, as they require to perform specific experiments. These parameters indicate the subject's fitness level, and as such, they are subject to variations. These two factors limit the scope of the model and the conclusions one can draw. In particular, the SoF model cannot be used to derive absolute measurements, but can be used only for relative comparisons between different scenarios.

IV. Energy Management System

The energy management system causally computes the motor torque based on available measurements. In determining the motor torque, we have to balance two objectives:

- **Charge Sustaining**: The bicycle is designed to operate within a bike sharing system; the reduction of the bicycle maintenance costs calls for an EMS that guarantees (if possible) that over the long run the battery pack is never discharged.
- **Effort Reduction**: The EMS needs to reduce the cyclist's effort with respect to a muscular bicycle given the same trip. Furthermore, in order for the cyclist to appreciate the effort reduction, the control system needs to yield a repeatable and predictable assistance. In fact, the first requirement of a usable human operated system is its predictability.

It is clear that these two objectives are conflicting. Given the charge sustaining objective, one cannot reduce the overall mechanical energy that the cyclist inputs at the pedal. It is however possible to exploit the metabolic efficiency gaps to reduce the cyclist's energy expenditure; or in other words, to improve her cycling efficiency.

To achieve this objective, we propose a hierarchical control algorithm. From the innermost, its three levels are:

- The maneuver assistance level: it generates the assistance torque based on the cyclist's inputs and road slope. The strategy exploits the cycling efficiency gaps in order to help the cyclist when the cycling efficiency is low and harvest energy when the cycling efficiency is higher.
- The battery power loop: the maneuver assistance level operates in open-loop from an energy standpoint; the battery power loop changes the maneuver assistance parameters to achieve a desired net battery power over the long run. This loop is adaptive and uses information collected on the specific cyclist.
- The SoC loop: the battery power loop operates at the power level, small tracking errors could lead to drift in the battery SoC, the State of Charge loop robustifies the energy balance by monitoring the actual SoC of the battery.

This multi-level approach allows the designer to separate the comfort related issues (dealt mainly by the maneuver assistance strategy), from the energy aspects (managed by the outermost layers); moreover, the nested approach of the two outermost loops simplifies the tuning procedure. Figure 6 graphically depicts the control architecture.

A. Maneuver assistance

The maneuver assistance level defines a nominal control logic for the torque generation and identifies a number of parameters the outer loop can change without modifying the main working principle of the assistance logic, thus yielding repeatability.

The nominal torque logic operates based on discrete types of maneuvers: $M = \{cruise, braking, start, downhill, uphill\}$.

The classification is based on the values of slope, bicycle velocity and the state of the freewheel. The freewheel is either engaged, when torque is being transmitted from the pedal to the wheel, or freewheeling when the cyclist is pedaling at a lower rate than that of the reduced wheel.

Given the considerations on the SoF model in Section III-D, the maneuver assistance strategy cannot be designed following model-based techniques, but rather it implements heuristics based on pedaling efficiency guidelines [8]:

1) Start maneuver: The start maneuver activates each time the freewheel engages at a speed below 7 km/h, independently of the slope state. The maneuver ends when either the speed of 10 km/h is reached or the freewheel disengages. This condition is a transient maneuver where pedaling efficiency is low. It is therefore beneficial that the motor provides assistance. The nominal assistance current level is $I_{nom_{start}}(v)$; Figure 7 depicts the current dependency on the bicycle speed. The curve is overlaid on the battery-to-wheel efficiency map. The figure shows that the current-velocity dependency tracks an iso-efficiency curve. The actual current level for the start maneuver is given by the nominal curve linearly scaled by the assistance level u_2:

$$I_{start}(v) = u_2 I_{nom_{start}}(v). \tag{5}$$

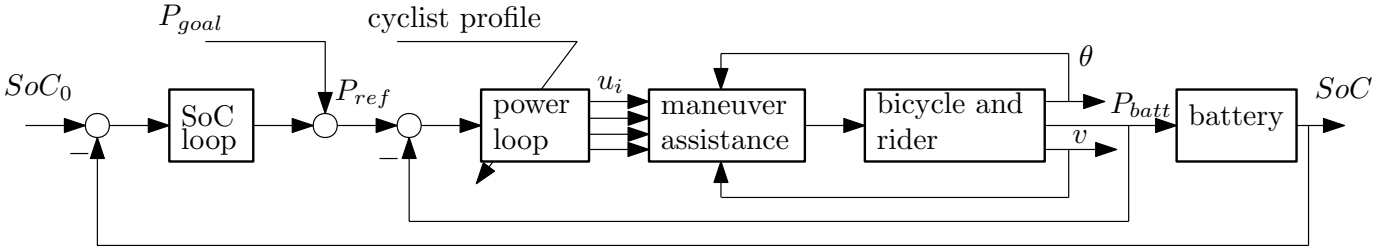

Fig. 6. Block diagram of the proposed control scheme.

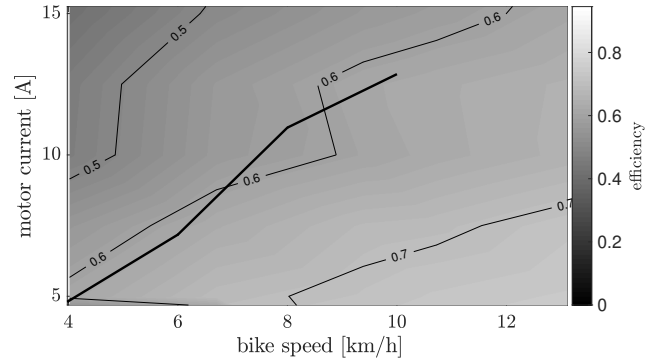

Fig. 7. Start maneuver nominal current as a function of bicycle speed and battery-to-wheel efficiency.

2) Braking maneuver: The braking maneuver is activated by the cyclist each time she back-pedals on flat road. Figure 8 plots the braking torque as a function of bike speed overlaid on the efficiency map. The design of the curve is a compromise between the efficiency objective and the requirement of sufficiently high braking force. The braking maneuver does not have any assistance level associated, as there is not reason to reduce the recovered energy with respect to the nominal case.

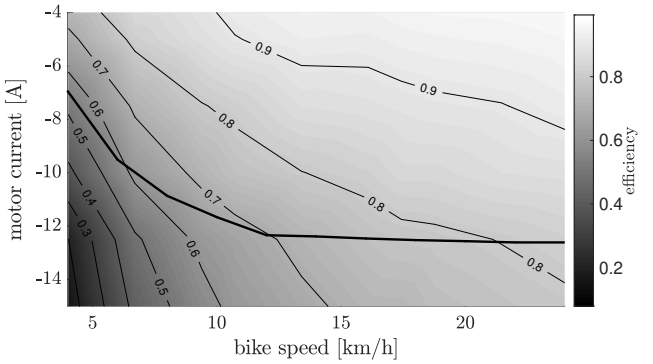

Fig. 8. Braking maneuver nominal current curve over pedal to battery efficiency.

3) Downhill/Uphill maneuver: The downhill maneuver triggers when the slope is negative ($\alpha < -1.25°$) and the start maneuver state is not active. Conversely, the uphill maneuver corresponds to a positive slope ($\alpha > 1.25°$) with an engaged freewheel and the start maneuver not active. The slope classification thresholds are compatible with the accuracy of the slope estimation algorithm implemented on the bicycle [15].

When cycling downhill, regenerative braking is always active in the attempt to maximize the regenerated energy. The level of regeneration depends on slope and velocity through a static map heuristically determined.

Conversely, when cycling uphill, the nominal assistance is

$$I_{slope}(v,\theta) = -\frac{(Mg\sin(\theta) + F_\mu(v))}{K_e r} \tag{6}$$

which represents a compensation of the gravitational force. The nominal assistance characteristic is then scaled through u_3 yielding

$$I_{uphill}(v,\theta) = u_3 I_{slope}(v,\theta). \tag{7}$$

4) Cruise maneuver: The cruise maneuver corresponds to having the freewheel engaged and cycling on a flat surface. It represents the condition when the cyclist is pedaling at constant medium-to-high speed. This condition is where most cyclists have their highest efficiency and it is thus a condition viable for regeneration.

The regeneration curve in this condition is more critical than in the previous cases. Here, the motor is actively working against the cyclist and, despite her high pedaling efficiency, the cyclist may not appreciate the instantaneous extra effort. For these reasons, we designed the nominal cruise regeneration curve, $I_{nom_{cruise}}(v)$, based on heuristics and cyclists' feedback. Figure 9 shows the resulting characteristic as a function of speed. One notes that:

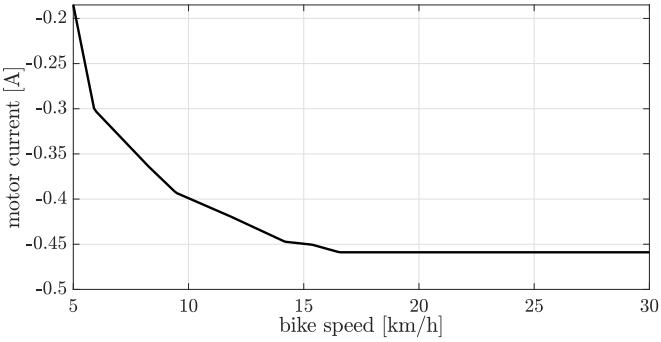

Fig. 9. Cruise maneuver nominal current curve.

- the regeneration level is smaller at low speed, where the friction resistance of the mechanical transmission is

higher and where the pedaling cadence is not comfortable for most cyclists.
- The regeneration is completely cut off below a threshold.
- The regeneration increases at high speed, corresponding to a more comfortable cadence.

The actual current is scaled by of u_1 and the regeneration is active only if the bike speed is above the value of the threshold u_4, resulting in:

$$I_{cruise}(v) = \begin{cases} u_1 I_{nom_{cruise}}(v) & if\ v \geq u_4 \\ 0 & if\ v < u_4. \end{cases} \tag{8}$$

Note that among the five maneuvers, three ($M_c = \{start, cruise, uphill\}$) are influenced by scaling parameters, we will call these controlled maneuvers; while two ($M_{uc} = \{braking, downhill\}$) are not scaled. These are the uncontrolled maneuvers. All the scaling variables have a minimum, u_k^{lb}, and maximum, u_k^{ub}, value; these limits are tuned according to comfort considerations.

B. Battery power closed loop

The maneuver assistance strategy makes sure that assistance and regeneration are active in the correct cycling phases and helps guaranteeing a predictable behavior of the assistance. Note however that

- the maneuver assistance strategy is open-loop from the energy perspective.
- It interfaces with the outer loop with 4 control variables, $\mathbf{u}(t) = \begin{bmatrix} u_1(t) & u_2(t) & u_3(t) & u_4(t) \end{bmatrix}$.

The battery power closed loop allocates the outer control variables u_k closing a loop on the average battery power so to track a desired value P_{ref}. As there are 4 control variables, the control problem is a Multiple Input Single Output problem. Designing controller for multiple inputs systems is challenging, we tackle this complexity with a model-based controller and control allocation strategy. The basis of this approach is a control-oriented model that describes the effect of each control variable u_k on the trip average power.

We derive the control-oriented model by considering a specific ride, indicated by the subscript j. Let's initially assume that the ride velocity, $v_j(t)$, slope, $\theta_j(t)$, and duration, $t_{ride,j}$, are known. We can compute the instantaneous battery power for each maneuver type, $i \in M$, as

$$P_{i,j}(t) = \frac{k_e I_j(t) \omega_j(t)}{\eta_j^\star} \sigma_i(t) \tag{9}$$

where

$$I_j(t) = I_{mot}(v_j(t), \theta_j(t), \mathbf{u}_j(t))$$

and $\sigma_i(t)$ is an activation variable that is 1 when maneuver i is active and 0 otherwise and does not depend on the control variables $\bar{u}$ but only on the ride characteristics. Note that in (9), $\eta^\star$ is an overall powertrain generalized efficiency that depends on the current and on the motor speed. For clarity of notation, through a small abuse of notation, the generalized efficiency is greater than 1 when the motor electrical power is negative.

Recalling the classification in controlled and uncontrolled maneuvers, we write the average power for ride j as:

$$\begin{aligned} \bar{P}_{batt,j} = \sum_{i \in M_c} \frac{\int_0^{t_{ride,j}} P_{i,j}(t) dt}{t_{ride,j}} + \\ + \sum_{i \in M_{uc}} \frac{\int_0^{t_{ride,j}} P_{i,j}(t) dt}{t_{ride,j}} + P_{load}. \end{aligned} \tag{10}$$

The power profiles associated to the uncontrolled maneuvers do not depend on the control variables, therefore their average power contributions, $\beta_{i,j}$, are insensitive to the control and constant. Conversely, the average powers associated to the controlled maneuvers depend on the control variables. By referring to $f_{i,j}$ as the average power associated to the maneuver i, one can thus write:

$$\begin{aligned} \bar{P}_{batt,j}(\mathbf{u}) = f_{cruise,j}(u_1(t), u_4(t)) + f_{start,j}(u_2(t)) + \\ f_{uphill,j}(u_3(t)) + \beta_{braking,j} + \beta_{downhil,j} + P_{load}. \end{aligned} \tag{11}$$

Note that, owing to the assistance maneuver strategy, u_1 and u_4 only affect the power associated to cruising; u_2 influences the start maneuver and u_3 the uphill contribution. To obtain the control-oriented model, we study the dynamics from the control variables to $\bar{P}_{batt,j}(\mathbf{u})$.

Starting from $f_{cruise,j}(u_1(t), u_4(t))$, one notes that it nonlinearly depends on the value of the control variables and the trip characteristics. To deal with this complexity, we describe the trip characteristics as random variables with two independent probability densities; p_v is the speed probability density limited to the cruise maneuver and p_σ is the probability for the cruise maneuver to be active. We recall that u_4 is the speed below which the controller stops regenerating while cruising. Therefore, the instantaneous regenerated power,

$$\tilde{P}_j(v, u_1) = \frac{k_e u_1 I_{nom_1}(v_j) \omega_j(v_j)}{\eta^\star_{cruise,j}},$$

becomes a function of the random variable v. We write the average of the cruising power as

$$\begin{aligned} & f_{cruise,j}(u_1, u_4) = \\ & = \frac{\int_v \int_0^{t_{ride,j}} \tilde{P}_j(v, u_1) p_{v,j}(v) p_{\sigma,j}(v_j) \mathbb{1}_{v > u_4} dt dv}{t_{ride,j}} = \\ & = \frac{\int_{u_4}^{\infty} \left(\int_0^{t_{ride,j}} \tilde{P}_j(v, u_1) p_{v,j}(v) p_{\sigma,j}(v) dt \right) dv}{t_{ride,j}}. \end{aligned}$$

The idea is to associate at each velocity its average power contribution in cruise, and then compute the overall average power by integrating over all velocities above u_4 (the only velocities contributing to the power) accounting for their probability of being reached in cruise. In order to simplify the parametrization of the speed density function, we assume it to be a gaussian with mean $\bar{v}_{cruise,j}$ and variance $\sigma^2_{cruise,j}$. Similarly, we approximate the cruise activation probability as uniform over speed: $p_{\sigma,j}(v) \simeq \rho_{cruise,j}$, with $\rho_{cruise,j} =$

$\frac{t_{cruise,j}}{t_{ride,j}}$ the proportion of time the cyclist actually spent in cruise; thanks to this assumption, we can write:

$$\begin{aligned} & f_{cruise,j}(u_1, u_4) = \\ =&\frac{\int_{u_4}^{\infty} \tilde{P}_j(v, u_1) p_{v,j}(v) \left(\int_0^{t_{ride,j}} p_{\sigma,j}(v) dt \right) dv}{t_{ride,j}} \simeq \\ =&\frac{\int_{u_4}^{\infty} \tilde{P}_j(v, u_1) p_{v,j}(v) \rho_{cruise,j} t_{ride,j} dv}{t_{ride,j}} = \\ =&\rho_{cruise,j} \int_{u_4}^{\infty} \tilde{P}_j(v, u_1) p_{v,j}(v) dv. \end{aligned}$$

Note that, strictly speaking, $\tilde{P}_j(v, u_1)$ depends on a time-varying efficiency; to avoid this additional complexity, in the derivation of the control-oriented model, we consider the average efficiency $\bar{\eta}^\star$.

The situation for $f_{start,j}(u_2(t))$ and $f_{uphill,j}(u_3(t))$ is less complex simpler. They also depend on the control variables and the trip characteristics, but the dependence of on u_2 and u_3 is linear due to the fact the the motor current linearly depends on u for all maneuvers as indicated in (5), (7) and (8).

We can therefore consider the following nonlinear control-oriented model that describes the average battery power for ride j:

$$\begin{aligned} \bar{P}_{batt,j}(\mathbf{u}) =& f_{cruise,j}(u_1, u_4) + \alpha_{2,j} u_2(t) + \\ &+ \alpha_{3,j} u_3(t) + \beta_{braking,j} + \\ &+ \beta_{downhill,j} + P_{load} \end{aligned} \tag{12}$$

where

$$\begin{aligned} \alpha_{2,j} =& \left. \frac{\partial f_{start}(u_2)}{\partial u_2} \right|_{\bar{u}} = \\ =& \frac{\int_0^{t_{ride,j}} k_e I_{nom_2,j}(t) \omega_j(t) \sigma_{start}(t) dt}{t_{ride,j}} \\ \alpha_{3,j} =& \left. \frac{\partial f_{uphill}(u_3)}{\partial u_3} \right|_{\bar{u}} = \\ =& \frac{\int_0^{t_{ride}} k_e I_{nom_3,j}(t) \omega_j(t) \sigma_{uphill}(t) dt}{t_{ride,j} \bar{\eta}_j^\star}. \end{aligned}$$

By linearizing $f_{cruise,j}(u_1(t), u_4(t))$ around the control value $\bar{\mathbf{u}}$, one obtains

$$\begin{aligned} \partial \bar{P}_{batt,j}(\mathbf{u}) =& \alpha_{1,j}(\bar{u}_4) \partial u_1 + \alpha_{2,j} \partial u_2 + \\ &+ \alpha_{3,j} \partial u_3 + \alpha_{4,j}(\bar{u}_1, \bar{u}_4) \partial u_4. \end{aligned} \tag{13}$$

where

$$\begin{aligned} \alpha_{1,j}(\bar{u}_4) =& \left. \frac{\partial f_{cruise,j}(u_1, u_4)}{\partial u_1} \right|_{\bar{u}} = \\ =& \rho_{cruise,j} \int_{\bar{u}_4}^{\infty} \frac{k_e I_{nom_1}(v) \omega(v)}{\bar{\eta}_j^\star} p_{v,j}(v) dv \\ \alpha_{4,j}(\bar{u}_1, \bar{u}_4) =& \left. \frac{\partial f_{cruise,j}(u_1, u_4)}{\partial u_4} \right|_{\bar{u}} = \\ =& -\rho_{cruise,j} \bar{u}_1 \frac{k_e I_{nom_1}(\bar{u}_4) \omega(\bar{u}_4)}{\bar{\eta}_j^\star} p_{v,j}(\bar{u}_4). \end{aligned} \tag{14}$$

The control sensitivities $\alpha_{k,j}$ describe how a variation of the control variables determines a variation of the average power. They depend on the linearization point (expressed in term of $\bar{\mathbf{u}}$) and a number of exogenous parameters that describe the specific ride properties. Thanks to the stochastic description of the ride, It is possible to summarize its energy characteristics in the following ride profiling vector:

$$\begin{aligned} \psi_j = [&\bar{v}_{cruise,j} \quad \sigma^2_{cruise,j} \quad \rho_{cruise,j} \quad \bar{\eta}_j^\star \quad \alpha_{2,j} \quad \alpha_{3,j} \\ &\beta_{braking,j} \quad \beta_{downhill,j}]^T. \end{aligned} \tag{15}$$

The above model still assumes the knowledge of the ride characteristics, but it parametrizes them in a compact way. Later on, the paper shows how to remove this assumption.

The power control loop exploits the control-oriented model in two phases: initialization, and power tracking.

1) Initialization: During the initialization phase (which happens when the cyclist reserves a bicycle through the app), the nonlinear model of the power expenditure and the cyclist profile determine the equilibrium value of the control variables by solving $\bar{P}_{batt,j}(\bar{\mathbf{u}}) = P_{ref}$, based on the nonlinear power model defined in (12) and on the reference computed by the State of Charge outermost loop. The initialization equation is under constrained as it depends on four control variables. We solve the nonlinear initialization equation iteratively: starting from an initial guess $\mathbf{u_0} = \begin{bmatrix} u_{1,0} & u_{2,0} & u_{2,0} & u_{3,0} & u_{4,0} \end{bmatrix}^T$, we sequentially compute the initial value of the control variables with Algorithm 1. In solving the equation, we adopt a

Algorithm 1 Initialization algorithm

```
ū = u_0
for i=1 to 4 do
    if ∃u_i : E[P̄_batt,j(ū_1:i−1, u_i, ū_i+1,4)] = P_ref then
        ū_i = u_1
        return ū
    end if
    P^lb = P̄_batt,j(ū_1:i−1, u_i^lb, ū_i+1,4)
    P^ub = P̄_batt,j(ū_1:i−1, u_i^up, ū_i+1,4)
    if |P^lb − P_ref| < |P^ub − P_ref| then
        ū_i = u_i^lb
    else
        ū_i = u_i^ub
    end if
end for
```

method inspired by the daisy chaining logic [33]. We define a priority ordering of the control variables and the algorithm achieves the desired battery power using the highest priority variable first. If modifying the highest priority variable cannot reach the objective, the algorithm saturates the highest priority variable to its maximum (or minimum) value and move to the next variable in the priority list. We defined the priority ordering through a series of heuristics: the order is mainly determined by the values of α_k, giving highest priority to the variables that have the largest control authority, with the only exception of u_4. α_4 is similar to α_1 but a variation of u_4, by changing an activation velocity, has a large impact on the predictability of the user experience. Based on this consideration, it has been given the lowest priority. The sequential method does not guarantee to find a solution, but

it has the advantage of running in real time on the bicycle electronics.

2) Power Tracking: The initialization is an open loop computation of the control variables based on two main assumptions: (1) the velocity profile and the probability of being in the cruise maneuver can be described by respectively a gaussian and a uniform probability densities and (2) the trip parameters are known apriori. The actual trip will very likely be different from the modeled one, and the open loop control will not guarantee the desired power tracking. To avoid this, while cycling, a closed loop controller determines the variation of the control variables based on the actual battery power and on the linearized model described by the control sensitivities $\alpha_{k,j}$.

We need to design a control for a MISO system, where the output is the battery power and the control inputs are the four control variables. Similarly to the initialization phase, the closed loop control is based on the daisy chaining approach. Each control variable u_k has a regulator R_k, and a priority level defined as before. At each instant, only the regulator with the highest priority which has not yet reached neither u_k^{lb} nor u_k^{ub} is active.

The control-oriented linearized model is the basis for the design of a model-based controller for each control action:

$$R_k(s) = \frac{1}{\alpha_{k,j}} \frac{I_k}{s} \frac{1}{\left(1 + \frac{s}{p}\right)}. \tag{16}$$

We tune each controller to achieve closed loop stability on the linearized model and a nominal bandwidth of 0.009 rad/s (equivalent to a settling time of about 10 minutes). The choice of a slow control is dictated by the fact that any sudden variation of the control variable is perceived as negative by the rider who would experience an unpredictable bicycle. In this context, having a model-based initialization of the controller is critical as it reduces the need to modulate the control variables during the ride.

3) User profiling: Both the initialization and the power tracking steps require the knowledge of the characteristics of the trip. These are, in general, not known a priori. However, bike sharing users tend to be creatures of habit. Most users use bike sharing as a *last mile* means of transportation to reach the main public transport hubs from their place of work or living and, the bicycles can be ridden in a constrained geographical area characterized by its topography and traffic patterns. In this scenario, the information needed to compute the control-oriented model and its control sensitivities do not considerably change from one trip to another (for the same user).

The idea is therefore that of creating and updating a profile of each user, storing the parametrization described in (15). After each ride of a user, we compute ψ_j based on the data of that ride, and the profile updated according to

$$\psi(k+1) = \gamma\psi(k+1) + (1-\gamma)\psi_j \tag{17}$$

where k is the ride index. We use $\gamma = 2/3$ to have a settling *time* of the filter of about 8 rides. At each ride, the EMS computes the control-oriented model based on the latest ψ, making it an adaptive EMS. Note that, in this context, the choice of parametrizing the velocity profile as a gaussian considerably reduces the data that has to be stored and transmitted at each rental.

C. State of Charge loop

The inner levels guarantee an accurate tracking of the requested power. However, power measurement errors may cause slow drifts in the state of charge. This makes it necessary to have an outer SoC controller. Thanks to the inner power loop, an integral controller, tuned on the closed-loop dynamics, and augmented with a feedforward action suffices. Figure 6 shows a schematic of the control architecture: the power reference depends on the current SoC and the desired SoC profile, as determined by a fleet-level management.

The main focus of this paper is the bicycle-level control (*i.e.* the State of Charge Loop); however an extensive and realistic validation of the EMS requires a reasonable SoC_0. Designing the fleet level manager is a complex task that needs to consider several aspects such as ride frequency, users price elasticity, maintenance costs and number of bicycles. In the following, with the objective to have a realistic reference to use for validation, we introduce a simple, yet realistic logic. In particular, we aim at achieving charge sustaining of the average state of charge of the fleet.

One could choose SoC_0 so to offset the energy lost during the previous idling period of the bicycle. This approach however leads to an uneven distribution of the effort among users, since the required energy would depend on the duration of the idling period of the bicycle being rented. A *fairer* approach is to operate at the daily level; the aim is to compensate the average energy loss during all idling periods of all bicycles. The average variation of SoC is

$$\overline{\Delta SoC_p} = \frac{-100}{Q_0}\left[P_{load}\left(1 - \frac{\nu}{24}\bar{t}_{ride}\right) + \bar{P}_{batt}\frac{\nu}{24}\bar{t}_{ride}\right]$$

where Q_0 is the total battery capacity, P_{load} is the idling power absorption of the sharing box, ν the average daily number of rides of the bike and $\bar{t}_{ride}$ the average ride duration. Imposing $\overline{\Delta SoC_p} = 0$, we obtain the recharging objective

$$\bar{P}_{goal} = -\frac{P_{load}\left(1 - \frac{\nu}{24}\bar{t}_{ride}\right)}{\frac{\nu}{24}\bar{t}_{ride}}.$$

The corresponding reference SoC to be tracked is:

$$SoC_0(t) = \frac{-1}{3.6Q}\bar{P}_{goal}t + SoC_{init} \tag{18}$$

where SoC_{init} is the SoC at pick up and t the time from the pick-up. Note that SoC_0 depends on the pick up frequency and it assumes a uniform pick up frequency.

Once the desired SoC profile is available, the State of Charge loop tracks it in closed loop.

V. Validation

The EMS validation considers several aspects. Using both simulations and experimental tests, we focus on the ability of the control system to track the required SoC_0 while helping the rider, and on the role of user profiling. Note that the

scope of our analysis is on the EMS at the bicycle level; we assume an average daily number of rides of $\nu = 3$, which is comparable with the one of existing passive bike sharing services [34]. The study of the EMS and its interaction with the fleet management is out of scope of this work; as a matter of fact, the proposed EMS will enable the development of the fleet management.

A. Simulation results

The simulation of the entire system provides a convenient way to exemplify the main features of the control system and quantify its effect on the cyclist's effort. The first set of simulations use the mission profile of Figure 10 which corresponds to a fit user. The figure also shows the distribution

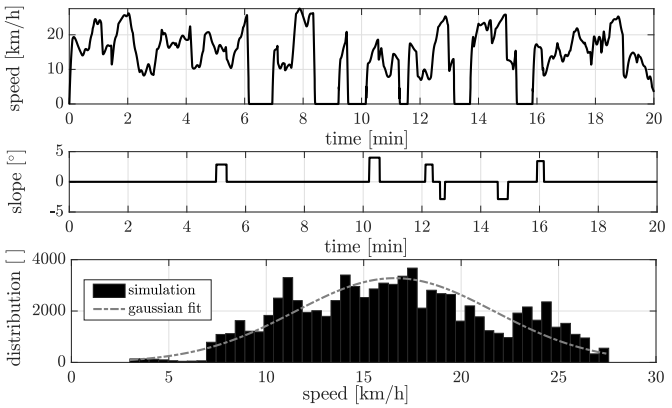

Fig. 10. Test mission profile generated by the trip generator: speed profile, slope profile and the speed distribution when in cruise maneuver.

of velocities during the cruise maneuver and its gaussian fit, which accurately describes the velocity distribution. Figure 11 plots the control variables behavior over the 20 minutes trip. The figure shows the ideal case of a perfect profiling: the

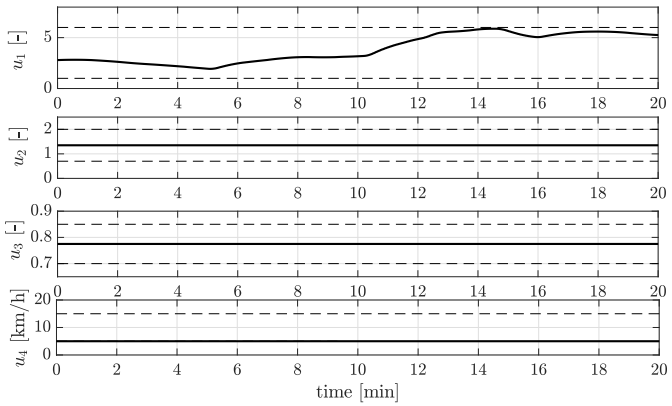

Fig. 11. Control variables trend over simulation test.

controller is using the trip parameters of that specific trip. Figure 12 plots the corresponding motor power and battery SoC. From figures, the following remarks are in order:

- despite the fact that the conditions are ideal, the controller is not using the full trip information, but only the cyclist's profiling.

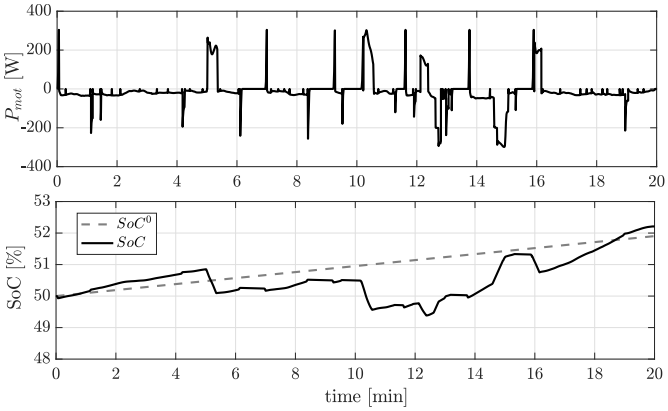

Fig. 12. State of Charge tracking over simulation test, the continuous line is the simulated value of State of Charge and the dashed line is the reference set-point.

- The daisy chain control allocation only needs to modulate u_1 as the other control variables are determined by the initialization. As u_1 never reaches its saturation limits, the other variables are not modulated. Note that u_1 varies smoothly.
- The desired battery SoC is tracked. Note that the objective is not a perfect instantaneous tracking of the reference as that would imply a lack of assistance.
- The motor power plot clearly shows that the motor provides assistance when needed. The small negative offset is the cruise maneuver contribution.

The previous simulations take advantage of an ideal profiling of the trip. The following simulations better quantify the impact of cyclist profiling. Profiling serves two goals: it initializes the power-loop and determines the controller gains to guarantee the desired bandwidth. We run a series of simulations considering multiple rental of the three types of users. The profile of each rider is initialized with the same level and updated with the algorithm described in the previous section using different rentals generated with the mission profile generator. Figure 13 plots the difference between the desired and the actual SoC at the end of each rental and the variance of u_1 during each rental (the first and therefore more used control variable in the daisy chaining approach). From figure, one notes that

- the tracking of the desired SoC improves as the profiling of the specific rider improves. While initially the EMS is not capable of reaching the desired SoC as it does not have enough information on the average trip; after 10 rentals, the EMS can guarantee the compensation of the average lost charge between rentals.
- The EMS tracks the desired SoC with progressively smaller variations of the control variables as the profiling vector converges. This is due to the initialization procedure.

These results indicate that the chosen profiling vector captures in an efficient way, the most relevant characteristics of the trip and that cycling profiling considerably improves the EMS performance.

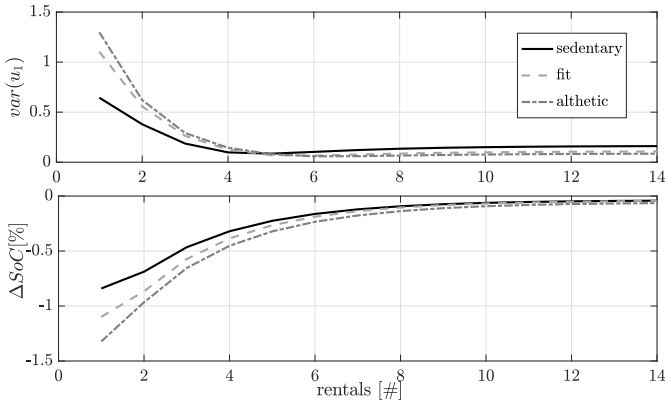

Fig. 13. Variance of u_1 and SoC tracking error at the end of each rental for three different types of users over 14 rentals.

Figures 14 and 15 further show the benefit of the cyclist profiling in the time domain. They depict the SoC and control variables behavior on the same trip, characterized by a steep ascent (up to 5°) with adaptive cyclist profiling and without. The time domain analysis confirms that cyclist profiling both

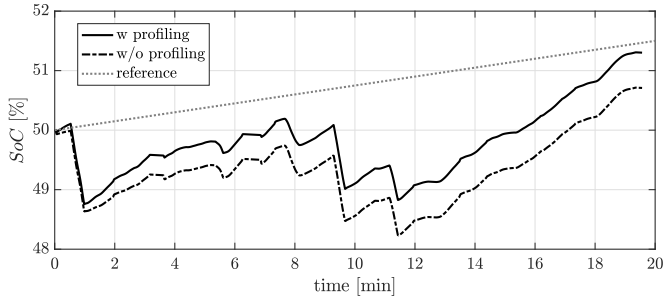

Fig. 14. SoC reference tracking during a single rental with steep incline. Comparison between the case with adaptive cyclist profiling and without.

improves the desired SoC tracking while at the same time yielding a more predictable cycling experience.

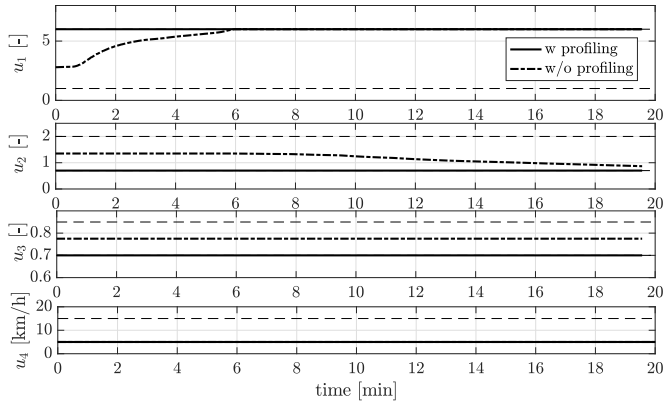

Fig. 15. Control variable during a single rental with steep incline. Comparison between the case with adaptive cyclist profiling and without.

The final set of simulations analyzes the cyclists' effort. Figure 16 plots the relative increment of the weighted state of fatigue and variance of the cyclist's torque when comparing a muscular bicycle against the hybrid bicycle with user profiling enabled. The figure considers 200 randomly generated trips executed by the three types of cyclists and computes the increment by repeating the same trip with the muscular and the hybrid bicycle. The fatigue model parameters are randomly generated for each cyclist considering nominal parameters for each cyclist type and adding a random variability of 10% at each run. We consider $MVC = 1000$ N, $k = 0.0153$ s^{-1}, and $R = 0.0063$ s^{-1} for the fit cyclist; $MVC = 1200$ N, $k = 0.0169$ s^{-1}, and $R = 0.0056$ s^{-1} for the athletic cyclist and $MVC = 800$ N, $k = 0.0192$ s^{-1}, and $R = 0.0047$ s^{-1} for the sedentary cyclist. The figure shows that the EMS

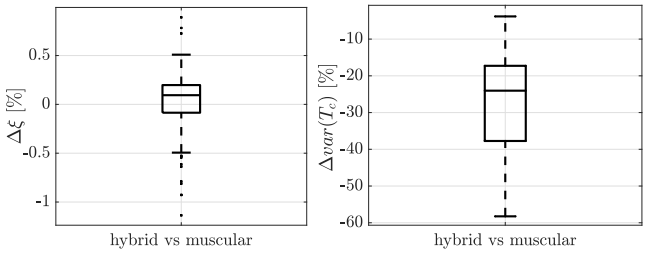

Fig. 16. Effort indices comparison for the same trip for a muscular bicycle and the hybrid bicycle.

can recharge the battery without an appreciable increment in cyclist's fatigue, while yielding a median reduction of 25% of the cyclist's torque variance. The EMS successfully shaves the pedaling torque peaks, considerably improving the cyclist's comfort and pedaling efficiency. The figure also shows that the State of Fatigue remains the same for both the muscular and hybrid bicycle. This result should be considered in the context of bike sharing; recall that each ride contributes to regenerating the average power lost during the idling periods. The fact that, despite recharging the battery of 2% over the trip, the fatigue does not increase indicates that the EMS is effective in improving the pedaling efficiency.

B. Experimental results

To experimentally validate the EMS, we implemented it locally on each bicycle on its onboard microcontroller; at the beginning and end of each rent, the bicycle communicates with the central server the user identification number and the ψ vector.

The experimental campaign refers to the data collected during the trials of the hybrid sharing free-floating service *bitride* tested in Milan between April and November 2018 [35]. Milan is a metropolitan area in Italy characterized by a relative flat terrain with slopes mainly due to overpasses and small hills. The main focus of the experimental analysis is the validation of the bicycle level EMS considering all the non-idealities that the model cannot quantify and the assessment of the user profiling algorithm on real data. We consider 13 rentals of a volunteer user. As expected, the specific user was quite regular in his rental habit; in particular, he picked and dropped the bicycle approximately in the same place for all his 14 rentals. Interestingly, the user's route crosses two overpasses. Figure 17 plots the velocity, slope and distribution of speed during the cruise maneuver of one of the 13 rentals

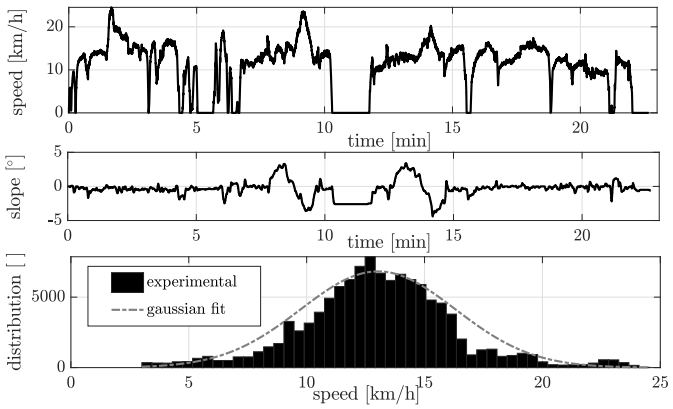

Fig. 17. Experimental ride input: speed profile, the slope profile and the distribution of speed during when the cruise maneuver is active.

Figure 18 plots the behavior of the iterative update of the cyclist profiling vector over the testing period. Note that, after

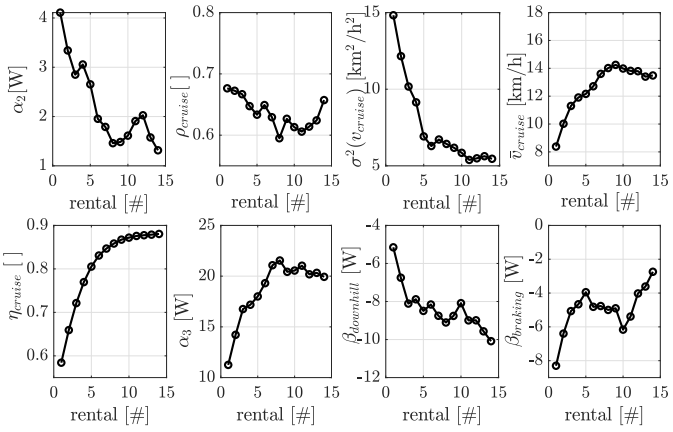

Fig. 18. Cyclist profiling vector evolution over 13 rentals of the same user.

around 10 rentals, the cyclist's parameters converge to their steady state, proving that the cycling style of the user is repeatable, of course within the possibilities of riding in a urban setting with traffic. Figure 19 shows the difference between the desired and the actual SoC at the end of each rental and the variance of u_1. As the profiling of the user converges and with it the controller adapts to a more accurate model of the system, the EMS needs to modulate the control variables less and the SoC objective is better achieved. As a matter of fact, starting from rental #6, the adaptation guarantees that the SoC tracking is achieved by only using u_1 and keeping the other control variables at their initial values.

Finally, Figure 20 plots the time evolution of the motor power and battery SoC in the last rental of the user. The figure shows that the bicycle, while still being recharged to compensate the loss of energy during idling, is capable of assisting the cyclist when he starts and accelerates and during the two overpasses.

VI. Conclusions

We propose a bicycle level EMS for a full hybrid bicycle designed to operate in a free-floating bike sharing system.

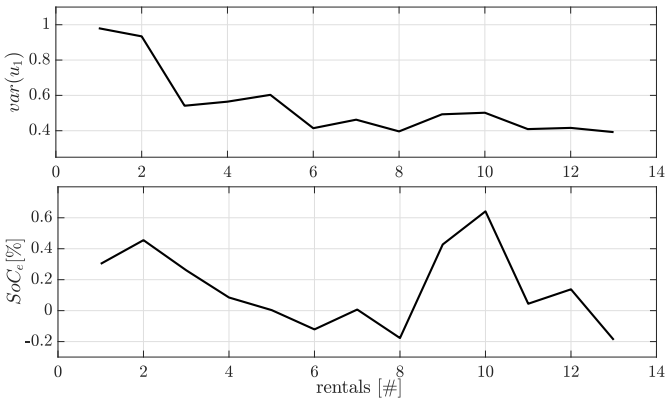

Fig. 19. Variance of u_1 and SoC tracking error at the end of each rental over 13 rentals of the same user.

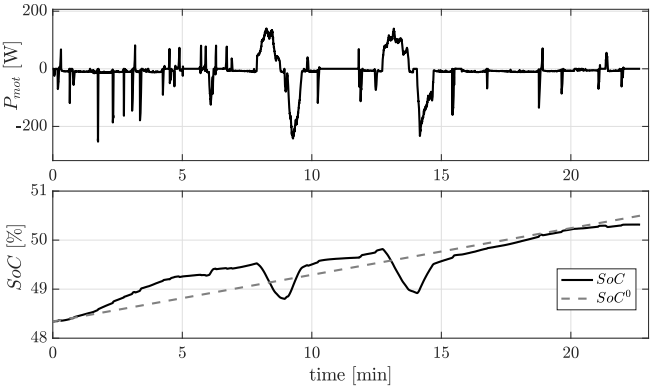

Fig. 20. Motor power and battery SoC tracking over an experimental test.

The energy management achieves three main objectives 1) it guarantees tracking of the desired SoC as determined by a fleet-level management strategy over a single rental 2) it provides assistance, improving the cycling experience, 3) it yields a natural cycling experience. We analyze the system in terms of a bike-sharing service and its peculiarities concerning mission profile, multi-user system and energy expenditure due to the communication and bicycle tracking.

The EMS is multi-layered. The innermost layer guarantees that the bicycle behavior is intuitive for the cyclist making sure that assistance is provided when needed and energy harvesting is used only during high efficiency pedaling. The middle level modulates the battery power based on an adaptive model of the cyclist and bicycle energy dynamics. The adaptive model is based on a user profiling. The outermost loop guarantees the SoC tracking increasing the robustness against power measurements offsets.

Extensive simulation and experimental campaigns validate this approach in terms of usability and desired SoC tracking. User profiling is paramount to provide assistance and, at the same time, avoid battery depletion of the bicycle battery. The proposed EMS can be used as the fundamental building block of an entire charge sustaining bicycle sharing system. Designing the charge sustaining system requires the development of the fleet level manager whose main task is the definition of

SoC_0 for each ride. The choice depends on several factors as pick-up distribution, rental frequency, maintenance costs and users demand. For example, the level of assistance and thus user acceptance of a free-floating electric bike sharing system depends on the number of bicycles and rentals per day. The higher the number of rentals, the less idling energy needs to be harvested during the rental and the higher the assistance can be. The interested reader is referred to [35] for a more detailed discussion at the fleet-level.

REFERENCES

[1] C. Kiefer and F. Behrendt, "Smart e-bike monitoring system: real-time open source and open hardware gps assistance and sensor data for electrically-assisted bicycles," *IET Intelligent Transport Systems*, vol. 10, no. 2, pp. 79–88, 2016.

[2] A. Mannion, H. Lhachemi, G. Russo, S. Sweeney, and R. Shorten, "On the design of cyber-physical control system for a smart pedelec (ebike)," in *2019 IEEE 58th Conference on Decision and Control (CDC)*. IEEE, 2019, pp. 2108–2113.

[3] S. Sweeney, R. Ordóñez-Hurtado, F. Pilla, G. Russo, D. Timoney, and R. Shorten, "A context-aware e-bike system to reduce pollution inhalation while cycling," *IEEE Transactions on Intelligent Transportation Systems*, vol. 20, no. 2, pp. 704–715, 2018.

[4] S. Cairns, F. Behrendt, D. Raffo, C. Beaumont, and C. Kiefer, "Electrically-assisted bikes: Potential impacts on travel behaviour," *Transportation research part A: policy and practice*, vol. 103, pp. 327–342, 2017.

[5] S. Reiss and K. Bogenberger, "Gps-data analysis of munich's free-floating bike sharing system and application of an operator-based relocation strategy," in *2015 IEEE 18th International Conference on Intelligent Transportation Systems*, Sep. 2015, pp. 584–589.

[6] P. Spagnol, M. Corno, R. Mura, and S. M. Savaresi, "Self-sustaining strategy for a hybrid electric bike," in *American Control Conference (ACC), 2013*, 2013, pp. 3479–3484.

[7] M. Corno, P. Giani, M. Tanelli, and S. M. Savaresi, "Human-in-the-loop bicycle control via active heart rate regulation," *IEEE Transactions on Control Systems Technology*, vol. 23, no. 3, pp. 1029–1040, 2014.

[8] M. Corno, D. Berretta, P. Spagnol, and S. M. Savaresi, "Design, control, and validation of a charge-sustaining parallel hybrid bicycle," *IEEE Transactions on Control Systems Technology*, vol. 24, no. 3, pp. 817–829, 2015.

[9] A. Sciarretta and L. Guzzella, "Control of hybrid electric vehicles," *IEEE Control Systems Magazine*, vol. 27, no. 2, pp. 60–70, 2007.

[10] G. Rizzoni, L. Guzzella, and B. M. Baumann, "Unified modeling of hybrid electric vehicle drivetrains," *IEEE/ASME transactions on mechatronics*, vol. 4, no. 3, pp. 246–257, 1999.

[11] G. Paganelli, S. Delprat, T.-M. Guerra, J. Rimaux, and J.-J. Santin, "Equivalent consumption minimization strategy for parallel hybrid powertrains," in *Vehicular Technology Conference. IEEE 55th Vehicular Technology Conference. VTC Spring 2002 (Cat. No. 02CH37367)*, vol. 4. IEEE, 2002, pp. 2076–2081.

[12] M. Corno, F. Roselli, and S. M. Savaresi, "Bilateral control of senza: A series hybrid electric bicycle," *IEEE Transactions on Control Systems Technology*, vol. 25, no. 3, pp. 864–874, 2016.

[13] J. Guanetti, S. Formentin, M. Corno, and S. M. Savaresi, "Optimal energy management in series hybrid electric bicycles," *Automatica*, vol. 81, pp. 96–106, 2017.

[14] M. El Lakkis, O. Sename, M. Corno, and D. B. Pietri, "Combined battery soc/soh estimation using a nonlinear adaptive observer," in *2015 European Control Conference (ECC)*. IEEE, 2015, pp. 1522–1527.

[15] M. Corno, P. Spagnol, and S. M. Savaresi, "Road slope estimation in bicycles without torque measurements," *Proc. 19th IFAC Word Congr*, pp. 6295–6300, 2014.

[16] P. Soden and B. Adeyefa, "Forces applied to a bicycle during normal cycling," *Journal of Biomechanics*, vol. 12, no. 7, pp. 527 – 541, 1979.

[17] A. Minetti, J. Pinkerton, and P. Zamparo, "From bipedalism to bicyclism: Evolution in energetics and biomechanics of historic bicycles," *Proceedings. Biological sciences / The Royal Society*, vol. 268, pp. 1351–60, 08 2001.

[18] M. Corno and G. Pozzato, "Active adaptive battery aging management for electric vehicles," *IEEE Transactions on Vehicular Technology*, 2019.

[19] J. Chavarren and J. Calbet, "Cycling efficiency and pedalling frequency in road cyclists," *European journal of applied physiology and occupational physiology*, vol. 80, no. 6, pp. 555–563, 1999.

[20] L. Pugh, "The relation of oxygen intake and speed in competition cycling and comparative observations on the bicycle ergometer," *The Journal of Physiology*, vol. 241, no. 3, pp. 795–808, 1974.

[21] Ø. Foss and J. Hallen, "The most economical cadence increases with increasing workload," *European journal of applied physiology*, vol. 92, no. 4-5, pp. 443–451, 2004.

[22] A. Belli and F. Hintzy, "Influence of pedalling rate on the energy cost of cycling in humans," *European journal of applied physiology*, vol. 88, no. 1-2, pp. 158–162, 2002.

[23] Ø. Foss and J. Hallén, "Cadence and performance in elite cyclists," *European journal of applied physiology*, vol. 93, no. 4, pp. 453–462, 2005.

[24] S. Fayazy, W. Nianfeng, S. Lucich, A. Vahidi, and G. Mocko, "Optimal Pacing in a Cycling Time-Trial Considering Cyclist's Fatigue Dynamics," in *American Control Conference, 2013*. IEEE, 2013, pp. 6457–6462.

[25] K. Isaacs, G. Glen, T. Mccurdy, and L. Smith, "Modeling energy expenditure and oxygen consumption in human exposure models: accounting for fatigue and EPOC," *Journal of Exposure Science and Environmental Epidemiology*, vol. 18, no. 3, pp. 289–298, 2007.

[26] P. Spagnol, G. Alli, C. Spelta, P. Lisanti, F. Todeschini, S. Savaresi, and A. Morelli, "A full hybrid electric bike: How to increase human efficiency," in *American Control Conference (ACC), 2012*, 2012, pp. 2761–2766.

[27] L. Ma, D. Chablat, F. Bennis, W. Zhang, and F. Guillaume, "A new muscle fatigue and recovery model and its ergonomics application in human simulation," *Virtual and Physical Prototyping*, vol. 5, no. 3, pp. 123–137, 2010.

[28] D. Imbeau, B. Farbos *et al.*, "Percentile values for determining maximum endurance times for static muscular work," *International journal of industrial ergonomics*, vol. 36, no. 2, pp. 99–108, 2006.

[29] L. Ma, D. Chablat, F. Bennis, and W. Zhang, "A new simple dynamic muscle fatigue model and its validation," *International Journal of Industrial Ergonomics*, vol. 39, no. 1, pp. 211–220, 2009.

[30] R. H. Morton, "The critical power and related whole-body bioenergetic models," *European journal of applied physiology*, vol. 96, no. 4, pp. 339–354, 2006.

[31] M. F. Bobbert, "Why is the force-velocity relationship in leg press tasks quasi-linear rather than hyperbolic?" *Journal of Applied Physiology*, vol. 112, no. 12, pp. 1975–1983, 2012.

[32] U. Emanuele and J. Denoth, "Power–cadence relationship in endurance cycling," *European journal of applied physiology*, vol. 112, no. 1, pp. 365–375, 2012.

[33] Zongli Lin and J. M. Berg, "Semi-global stabilization of linear systems with position and rate limited actuators in daisy chain," in *Proceedings of the 37th IEEE Conference on Decision and Control (Cat. No.98CH36171)*, vol. 2, Dec 1998, pp. 1979–1980 vol.2.

[34] "Mobike touts bike-sharing scheme in LatAm," http://www.chinadaily.com.cn/world/2017-12/03/content_35180185.htm, accessed: 2020-01-04.

[35] A. Duz, M. Corno, and S. M. Savaresi, "Is charge sustaining achievable in electric free-floating bicycle sharing?" in *2020 IEEE Intelligent Transportation Systems Conference (ITSC)*. IEEE, 2020, pp. 1955–1960.